Inverse Patch Transfer Function With Fast Iterative Shrinkage-Thresholding Algorithm as a Tool for Sparse Source Identification

LINGYU LOU[1], ZHONGMING XU[1,2], LINSEN HUANG[1], ZHIFEI ZHANG[1], AND YANSONG HE[1]
[1]College of Automotive Engineering, Chongqing University, Chongqing 400044, China
[2]State Key Laboratory of Mechanical Transmission, Chongqing University, Chongqing 400044, China

Corresponding author: Zhongming Xu (xuzm@cqu.edu.cn)

ABSTRACT Inverse patch transfer functions (iPTF) method is an efficient technique for sound field reconstruction and separation of arbitrarily shaped sound sources in noisy acoustic environments. By applying Neumann boundary condition to a closed virtual cavity surrounding the source, the Helmholtz integral equation is simplified and can be solved with a Green's function satisfying the Neumann boundary condition. However, in the identification of sparsely distributed sources, ghost sources appear in the result solved by using the iPTF method with classic Tikhonov regularization methods and influence the accuracy of identification. In the present work, an evanescent Green's function with fast convergence of calculation is utilized, and a technique that combines the iPTF method and Fast Iterative Shrinkage-Thresholding Algorithm aimed at improving the performance for the identification of sparsely distributed source is proposed. Then double layer measurements, instead of using expensive p-u probes, are employed to acquire the normal velocity of the hologram surface. In numerical simulations, the normal velocities of two anti-phased piston sources are well reconstructed with high sparsity while a disturbing source is radiating in the sound field within the frequency band of 50 to 1000 Hz. Finally, an experiment on two baffled loudspeakers has been carried out. The results of simulations and experiments indicate that the proposed technique has obviously improved the accuracy of the iPTF method in the identification of sparsely distributed sources for the frequency band from 50 to 1000 Hz.

INDEX TERMS Acoustic source identification, fast iterative shrinkage-thresholding algorithm, Green's function.

I. INTRODUCTION

Near-field acoustic holography (NAH) has been developed and used for the identification of sound sources and reconstruction of sound field through near-field measurements. First proposed by Williams [1] and Maynard [2], NAH performs a 2D spatial Discrete Fourier Transform on the Helmholtz equation to identify the source velocity on a rectangular surface. However, the NAH based on DFT is limited to the identification of regularly shaped sources such as planar and cylindrical surfaces. To identify irregularly shaped sources that are pretty common in industrial applications,

The associate editor coordinating the review of this manuscript and approving it for publication was Huawei Chen.

the inverse Boundary Element Method (iBEM) [3], [4] has been proposed. The application of iBEM is limited by its heavy computational cost. An alternative approach to iBEM is the equivalent source method (ESM) [5], [6]. In the ESM, the arbitrarily shaped sources are replaced by a set of equivalent sources whose strength remains to be solved. In the meanwhile, other NAH techniques such as Helmholtz equation least squares method (HELS) [7], statistically optimized near-field acoustical holography (SONAH) [8]–[10] have been developed. The NAH techniques mentioned above usually are performed in an anechoic room which is not suitable in industrial environment. Thus it is necessary to take the noisy environment, where disturbing sources and reflection from walls exists, into consideration.

To identify sources with an arbitrary structure in non-anechoic environment efficiently, the inverse patch transfer function method (iPTF) has been proposed [11]–[13]. During the process of the iPTF method, the disturbing sources will be eliminated. Different from other NAH techniques, the iPTF method reconstructs the sound field with a high resolution by identifying the normal velocity of sound sources [13]. A key process of the iPTF method is to calculate the patch transfer function with the Green's function of an enclosed volume fulfilling specific boundary conditions. Different iPTF methods can be developed if different boundary conditions are applied to the virtual volume boundary. Forget developed two iPTF methods [14] which use uniform boundary conditions (Neumann) and mixed boundary conditions (Neumann and Dirichlet) respectively. Xiang [15] presented an evanescent Neumann Green's function for a cuboid cavity. The evanescent Neumann Green's function matches the property of evanescent acoustic waves and shows better convergence than the classic Neumann Green's function in which the decay of acoustic waves is not considered.

The iPTF methods are ill-posed problems as all inverse problems in acoustics. To stabilize the solution, regularization methods are required. Among the regularization methods, Tikhonov regularization [16] has been widely studied and truncated singular value decomposition (TSVD) is also used in iPTF methods. Williams [17] studied several regularization methods and parameter selection procedures for NAH. Totaro [12] proposed an adapted parameter selection strategy combining the classic L-curve and acoustic power conservation to address the problem that the L-curve strategy fails at some frequencies. However, when identifying sparsely distributed sources the reconstruction accuracy is affected by the ghost sources, which is associated with the real sources. Recently, l_1-norm-based regularization has been widely studied due to its capability to provide a sparse solution. Hald proposed the wideband acoustic holography (WBH) [18] combining the gradient iteration algorithm and a dynamic filter process to enforce the sparsity. Hald [19] also compared several sparse equivalent source methods for NAH such as ISTA [20] and IRLS [21]. Among the ℓ_1 regularization methods, the fast iterative shrinkage-thresholding algorithm (FISTA) [22] proposed by Beck gains great popularity due to its efficiency and generality.

In this paper, a technique that introduced the idea of FISTA into the iPTF method is presented for the identification of sparsely distributed sources. In addition, double layer pressure measurements are utilized instead of single layer measurements with p-u probes because microphones are more widely used in NAH than p-u probes which are pretty expensive. In section II, the basic theory of the iPTF method and FISTA is described. Two baffled piston sources in a noisy environment are used in Section III for numerical validation. Then in Section IV, an experiment is conducted to validate the technique. Finally, several conclusions are presented in Section V.

II. THEORY

A. THEORETICAL BACKGROUND OF THE INVERSE PATCH TRANSFER FUNCTION METHOD

Fig. 1 gives an example of the iPTF method. A vibrating surface S_v radiates with a normal velocity v_k in a noisy environment, where reflective waves and disturbing sources exist. Assume that the vibrating surface S_v and virtual surface S_c delimits a virtual cavity Ω_i. The point Q is located on the vibrating surface S_v and Q' is located on the virtual surface S_c. Moreover, there are disturbing sources outside the virtual cavity Ω_i but inside the cavity Ω_0. The pressure $p(Q')$ can be obtained by solving the Helmholtz integral equation:

$$\alpha p(Q') = \iint_{S_c \cup S_v} \left(G(Q, Q') \frac{\partial p(Q)}{\partial n} - p(Q) \frac{\partial G(Q, Q')}{\partial n} \right) dS \quad (1)$$
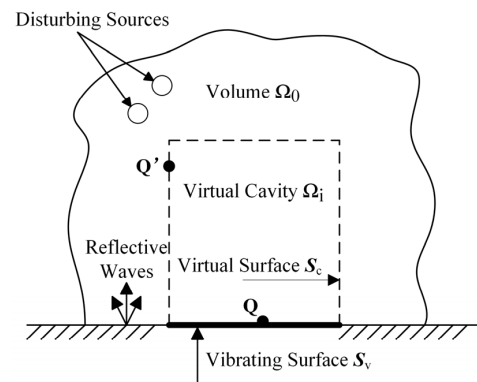

FIGURE 1. Definition of the virtual volume Ω_i and virtual surface S_c.

where $p(Q)$ is the pressure on the boundary of the virtual cavity, $G(Q, Q')$ denotes the Green's function, and $\partial/\partial n$ represents the exterior normal derivative to the boundary. The coefficient α denotes the solid angle, which is 0 for a point outside the volume Ω_i, 1/2 for a point on the boundary surface of the virtual cavity and 1 for a point inside the volume Ω_i. It is worth noting that the boundary condition which the Green's function satisfies can be arbitrarily chosen because it applies only to $G(Q, Q')$, not to $p(Q)$. That is to say, the arbitrary virtual boundary conditions are mathematical tools for solving the problem. In the present work, the Green's function satisfies the Neumann boundary condition:

$$\frac{\partial G(Q, Q')}{\partial n} = 0, \quad \forall Q \in S_c \cup S_v, \quad (2)$$

Additionally, Euler's equation is written as

$$\frac{\partial p(Q)}{\partial n} = -i\rho_0 ck v(Q), \quad (3)$$

where $v(Q)$ is the normal velocity. By using Equations (2) and (3), Equation (1) can be written as

$$p(Q')$$
$$= -2i\rho_0 ck \int_{S_c \cup S_v} G(Q, Q') v(Q) dS$$
$$= -2i\rho_0 ck \left(\int_{S_v} G(Q, Q') v(Q) dS_v + \int_{S_c} G(Q, Q') v(Q') dS_c \right)$$
$$\quad (4)$$

Then Equation (4) needs to be written in a discrete form for numerical calculation. The virtual surface and source surface are meshed into small elements called patches and Equation (4) will be written as

$$p_m = -2i\rho_0 ck \sum_{j=1}^{N} \left(G(Q_j, Q')v(Q_j)\Delta S_j \right)$$

$$-2i\rho_0 ck \sum_{i=1}^{M} \left(G(Q_i, Q')v(Q_i)\Delta S_i \right) \quad (5)$$

where M, N are the numbers of patches on the vibrating surface and virtual surface respectively. p_m represents the pressure $p(Q')$ at the mth point of the virtual surface, ΔS_j, ΔS_i denotes the area of the patch. Equation (5) can be rewritten as a matrix form as:

$$\mathbf{p}_m = \mathbf{Z}_{mj}\mathbf{v}_j + \mathbf{Z}_{mi}\mathbf{v}_i \quad (6)$$

where $\mathbf{Z}_{mj}$ and $\mathbf{Z}_{mi}$ are defined as follows:

$$\mathbf{Z}_{mj} = -2i\rho_0 ckG(Q_j, Q')\Delta S_j \quad \text{and} \quad \mathbf{Z}_{mi}$$
$$= -2i\rho_0 ckG(Q_i, Q')\Delta S_i \quad (7)$$

Equation (6) establishes the relationship between the pressure of the virtual surface and normal velocity of the vibrating surface. $\mathbf{Z}_{mj}$ (resp. $\mathbf{Z}_{mi}$) is the impedance matrix representing the transfer function between the average pressure of the patch m and average velocity of the patch j(resp. i). Finally, the normal velocity of the vibrating surface can be solved by inverting Equation (6):

$$\mathbf{v}_j = \mathbf{Z}_{mj}^{-1} \left(\mathbf{p}_m - \mathbf{Z}_{mi}\mathbf{v}_i \right) \quad (8)$$

Normal velocities $\mathbf{v}_i$ and pressure $\mathbf{p}_m$ of the virtual surface which is also the measurement surface require to be obtained by p-u probes or double pressure measurements which will be illustrated in section II-C. The impedance matrix will be evaluated through the Green's function satisfying the specific boundary condition which will be explained in section II-B. After the velocity of the vibrating surface is solved, the sound field around the source can be reconstructed through the Rayleigh's integral.

B. NEUMANN EVANESCENT GREEN'S FUNCTION

Green's functions provide a concise mathematical tool for acoustic radiation problems. As mentioned before, the Green's function used in this paper satisfies the Neumann boundary condition. It is known that the sound wave propagates as an evanescent wave rather than as a propagation wave. So it is more suitable to select the evanescent Green's function instead of the classic Green's function [15], [23]. The evanescent Green's function matches the property of evanescent waves that wave decays in an exponential form with the distance from the sound source. The evanescent Green's function used can be written as:

$$G(\overrightarrow{r}, \overrightarrow{r_0}) = \sum_{t,u=0}^{\infty} g_{tu}(z, z_0)\psi_{tu}(x, y)\psi_{tu}(x_0, y_0) \quad (9)$$

$$\psi_{tu}(x, y) = \frac{4}{(1 + \delta_{t0})(1 + \delta_{u0})l_x l_y} \cos \frac{t\pi x}{l_x} \cos \frac{u\pi y}{l_y} \quad (10)$$

$$g_{tu}(z, z_0) = \begin{cases} -\dfrac{\cos\left[k_{ztu}(l_z - z_0)\right]\cos(k_{ztu}z)}{k_{ztu}\sin(k_{ztu}l_z)}, & \text{if } z \le z_0 \\[3mm] -\dfrac{\cos\left[k_{ztu}(l_z - z)\right]\cos(k_{ztu}z_0)}{k_{ztu}\sin(k_{ztu}l_z)}, & \text{if } z_0 \le z \end{cases} \quad (11)$$

$$k_{ztu} = \sqrt{k^2 - [(\frac{t\pi}{l_x})^2 + (\frac{u\pi}{l_y})^2]} \quad (12)$$

where l_x, l_y, and l_z are the sizes of the virtual volume, δ_{t0}, δ_{u0} are the Kronecker delta.

C. DOUBLE LAYER PRESSURE MEASUREMENTS

To solve Equation (8), pressure $\mathbf{p}_m$ and particle velocities $\mathbf{v}_i$ of the virtual surface must be obtained with p-u probes that are costly and difficult to calibrate. Thus another method named double layer pressure measurements, which only require the lower-priced microphones, are introduced. As shown in Fig. 2 and Equation (13), pressure measurements are taken on two close hologram surfaces S_1 and S_2, then the pressure p_0 of the middle surface S_0 can be calculated as the average of the pressure p_1 and p_2, while the normal velocity v_n of the middle surface can be calculated:

$$p_0 \approx \frac{p_1 + p_2}{2} \quad (13)$$

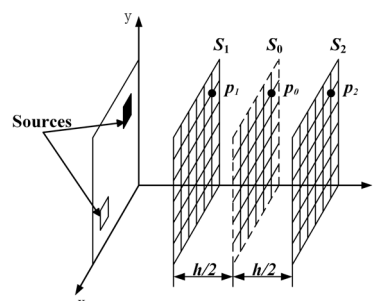$$v_n \approx -\frac{1}{i\rho_0 ck}\frac{p_2 - p_1}{h} \quad (14)$$

FIGURE 2. Definition of double layer pressure measurements.

D. TIKHONOV REGULARIZATION

In Equation (8), the inversion of the impedance matrix $\mathbf{Z}_{mj}$ which is ill-conditioned is required to reconstruct the velocity field of the source. Equation (6) can be rewritten in the form of $\mathbf{Ax} = \mathbf{b}$ which is classical in acoustics [16], [24]:

$$\mathbf{Z}_{mj}\mathbf{v}_j = \mathbf{p}_i \quad \text{with } \mathbf{p}_i = \mathbf{p}_m - \mathbf{z}_{mi}\mathbf{v}_i \quad (15)$$

Tikhonov regularization is frequently used in the iPTF method to address the ill-posed problem. The principle of Tikhonov regularization is to generate a solution by making a compromise between the solution norm $\left\|\mathbf{v}_j\right\|_2$ and the residual norm $\left\|\mathbf{p}_i - \mathbf{Z}_{mj}\mathbf{v}_j\right\|_2$:

$$\underset{\mathbf{v}_j}{\text{minimize}} \left\|\mathbf{p}_i - \mathbf{Z}_{mj}\mathbf{v}_j\right\|_2^2 + \lambda \left\|\mathbf{v}_j\right\|_2^2 \quad (16)$$

where $\|\cdot\|_2^2$ is the λ_2 norm, λ denotes the regularization parameter. Then a simple analytic solution can be obtained:

$$\mathbf{v}_j = \left[\mathbf{Z}_{mj}^H \mathbf{Z}_{mj} + \lambda \mathbf{I} \right]^{-1} \mathbf{Z}_{mj}^H \mathbf{p}_i \tag{17}$$

where $\mathbf{I}$ represents the unit diagonal matrix, H is the Hermitian transpose. Selecting an optimum regularization parameter λ is the most crucial process in the Tikhonov Regularization. In the iPTF method, L-curve, as well as Generalized Cross Validation (GCV), is frequently used among the techniques for the regularization parameter selection. L-curve is used in the present work for comparison with the proposed technique.

E. THE FAST ITERATIVE SHRINKAGE-THRESHOLDING ALGORITHM

Lately, ℓ_1-norm-based regularization has been widely studied due to its capability to give satisfactory sparse solutions under sparse conditions. Among the ℓ_1 norm regularization methods, the Fast Iterative Shrinkage-Thresholding Algorithm (FISTA) is widely studied due to its simplicity and generality. In this paper, the ideas of the FISTA and a filter process is introduced to suppress the ghost source. According to the theory of ℓ_1 norm regularization, the inverse problem related to Equation (6) can be redefined as:

$$\underset{\mathbf{v}_j}{\text{minimize}} \ \frac{1}{2} \left\| \mathbf{Z}_{mj} \mathbf{v}_j - \mathbf{p}_i^2 \right\|_2^2 + \lambda \left\| \mathbf{v}_j \right\|_1 \tag{18}$$

Varying with the Tikhonov regularization, Equation (18) is solved using an iterative process due to the lack of an analytic solution. And there are no regularization selection techniques like L-curve and GCV in Tikhonov regularization. In order to get the solution, an iterative proximal gradient-based method is applied. Initializing $\mathbf{v}_j^0$ with an approximating solution $\mathbf{v}_{tik}$ using Tikhonov regularization, $\mathbf{y}^1 = \mathbf{v}_j^0$, $t^1 = 1$. Its iterative formula is given as

$$\mathbf{v}_j^{n+1} = \text{prox}_{\frac{1}{L}\lambda}(\mathbf{y}^n - \nabla F(\mathbf{y}^n)/L) \tag{19}$$

$$t^{n+1} = \frac{1}{2}(1 + \sqrt{1 + 4(t^n)^2}) \tag{20}$$

$$\mathbf{y}^{n+1} = \mathbf{v}_j^n + ((t^n - 1)/t^{n+1})(\mathbf{v}_j^n - \mathbf{v}_j^{n-1}) \tag{21}$$

where ∇F is the gradient function as shown in Equation (22), L is the Lipchitz constant of ∇F which equals to maximum eigenvalue of $\mathbf{Z}_{mj}^H \mathbf{Z}_{mj}$

$$\nabla F(\mathbf{y}) = 2\mathbf{Z}_{mj}^H(\mathbf{Z}_{mj}\mathbf{v}_j - \mathbf{p}_i) \tag{22}$$

Moreover, a filter process is used to remove ghost sources and improve the robustness of the capability to suppress ghost sources. All elements in $\mathbf{v}_j^{n+1}$ below a certain threshold are set to zero:

$$\mathbf{v}_j^{'n+1,i} = \begin{cases} \mathbf{v}_j^{n+1,i} & \text{if } \left| \mathbf{v}_j^{n+1,i} \right| \geq T_n \\ 0 & \text{otherwise} \end{cases} \tag{23}$$

where T_n is the threshold updated during the iteration expressed as

$$T_n = \frac{1}{D_n/10 + 1} e^{-D_n/10} \left| \mathbf{v}_j^{n+1}, \text{max} \right| \tag{24}$$

$$D_{n+1} = D_n + \Delta D \tag{25}$$

Because T_n in Equation (24) is in an exponential form, the results will converge smoothly and quickly. Most of the ghost sources will be removed at the first few steps in the iteration if D_0 is given small value, whereas the capability of removing ghosting sources will be weakened when D_0 is too large. The value of ΔD influences the continuity of T_n. Some ghost sources that need to be suppressed may be ignored if it is too large. The following values are found to work well in most cases: $D_0 = 1$, $\Delta D = 0.01$ and $D_{\text{max}} = 30$. The regularization parameter can be selected by [19]:

$$\lambda = 1.16 s_{\text{max}} 10^{-D/20} \|\mathbf{p}_i\|_2 / \sqrt{I} \tag{26}$$

where s_{max} is the largest singular value of $\mathbf{Z}_{mj}$, and I is the number of columns of $\mathbf{Z}_{mj}$.

The iteration process is stopped when:

$$D_{n+1} > D_{\text{max}} \text{or} \left\| \nabla F \left(\mathbf{v}_j^{n+1} \right) \right\|_2 \leq \varepsilon \left\| \nabla F \left(\mathbf{v}_j^0 \right) \right\|_2 \tag{27}$$

Once the iteration process is stopped, a sparse and precise estimation of normal velocities on the vibrating surface v_k^{n+1} is obtained.

The procedure of the iPTF method with FISTA for sparse source identification can be described as follows:

Begin

Calculate the impedance matrices $\mathbf{Z}_{mj}$ and $\mathbf{Z}_{mi}$ using Neumann evanescent Green's function;

Compute the pressure $\mathbf{p}_m$ and particle velocities $\mathbf{v}_i$ of the virtual surface through double layer pressure measurements;

Set $D_0 = 1$, $\Delta D = 0.01$ and $D_{\text{max}} = 30$, compute s_{max}, λ;

Initialization: $n = 1$, $\mathbf{v}_j^0 = \mathbf{v}_{tik}$ $\mathbf{y}^1 = \mathbf{v}_j^0$, $t^1 = 1$;

While $D_{n+1} \leq D_{\text{max}}$ or $\left\| \nabla F \left(\mathbf{v}_j^{n+1} \right) \right\|_2 > \varepsilon \left\| \nabla F \left(\mathbf{v}_j^0 \right) \right\|_2$

Compute $\mathbf{v}_j^{n+1}$, t^{n+1}, $\mathbf{y}^{n+1}$, $\nabla F(\mathbf{y})$;

if $\left| \mathbf{v}_j^{n+1,i} \right| \geq T_n$

Set $\mathbf{v}_j^{n+1,i} = 0$;

end

n = n+1;

Output the identified solution $\mathbf{v}_j$;

End

III. NUMERICAL VALIDATION
A. DESCRIPTION OF THE SIMULATION MODEL

To validate the capabilities of the iPTF method with FISTA for the identification of sparse sources, numerical simulations are carried out. As shown in Fig. 3 (a), two piston sources (0.05 $m \times$ 0.05 m) driven in antiphase in a large baffle are selected for the identification. In simulations, the normal velocities to be identified of the piston sources are constant with a value of 0.01 m/s. After that, a virtual rectangular volume (0.45 $m \times$ 0.45 $m \times$ 0.05 m) is defined surrounding the
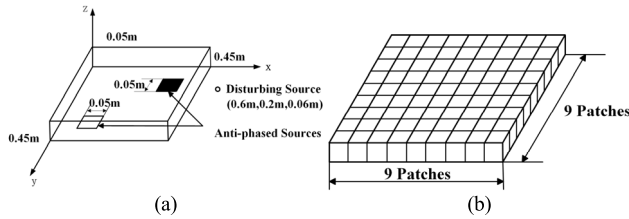
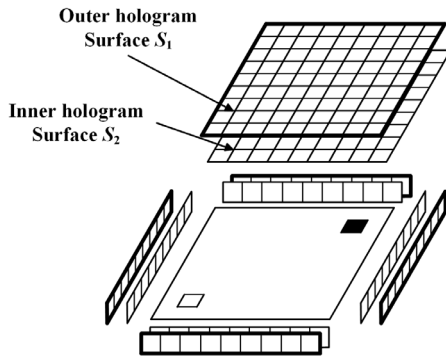**FIGURE 3.** (a) Model of anti-phased sources (b) mesh of measurement surfaces.

FIGURE 4. All hologram surfaces required for double layer pressure measurements.

piston sources. A disturbing monopole source is radiating from the location of $(0.5, 0.3, 0.05)$ *m* near the cavity. Then, the identification surface $(0.45\ m \times 0.45\ m)$ is meshed into 81 identical patches (9×9), while the boundary surfaces of the cavity are meshed into 117 patches in total including 81 identical patches (9×9) on of top surface and 9 patches of each side surface (9×1) as illustrated in Fig. 3 (b). As illustrated in Section II-C, the sound pressure and particle velocity on the measurement surfaces are acquired through double layer pressure measurements. Thus the sound pressure at the center of each patch on the outer and inner hologram surface needs to be obtained first as shown in Fig. 4. Then, the sound pressure and particle velocity on the virtual surfaces can be calculated by Equations (13) and (14). Here, the distance h between the two hologram surfaces S_1 and S_2 is set as $0.03\ m$. As mentioned in Section II, the boundary condition applied to the surfaces of the virtual cavity in simulations is Neumann boundary condition.

B. THE CONDITION NUMBER OF THE ILL-CONDITIONED IMPEDANCE MATRIX

The impedance matrix $\mathbf{Z}_{mj}$ establishes the relationship between normal velocities of the source surface and sound pressure of the virtual surfaces. The inversion of $\mathbf{Z}_{mj}$ is unavoidable in the process of identification. Thus the ill-conditioning level of $\mathbf{Z}_{mj}$ will affect the reconstruction accuracy. The condition number κ which identifies the level of ill-conditioning is defined as

$$\kappa(\mathbf{Z}_{mj}) = \frac{\sigma_{\max}}{\sigma_{\min}} \qquad (28)$$

where $\sigma_{\min}$ and $\sigma_{\max}$ are the smallest and biggest singular values of $\mathbf{Z}_{mj}$ respectively.

The condition number is affected by many factors, such as the size of the volume, the Green's function and the number of virtual cavity modes extracted. Here, the influence of the modal truncation on the condition number will be discussed. In fact, Ouisse [25] pointed out that the number of virtual cavity modes in a direction has to be no fewer than the exact number of patches in that direction. Fig. 5 shows the condition number of the impedance matrix $\mathbf{Z}_{mj}$ with different orders of modes truncated. It is obvious that the condition number with different orders of modes fluctuates and the curves peak at the eigenfrequencies of the virtual volume. It is obvious that the condition number of impedance matrix with 8×8 modes is much larger than others. The other three curves in Fig. 5 almost overlapped which means that the level of ill-conditioning of them is the same. In this paper, the order of the virtual cavity modes is set as 18×18 in simulations.
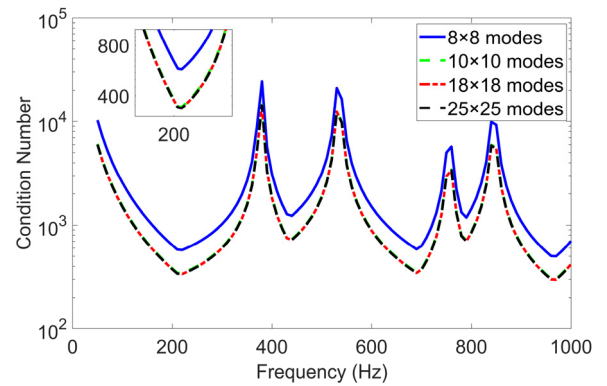

FIGURE 5. Influence of evanescent wave expansions on the condition number of Patch impedance matrices for a virtual cavity of 0.45 m × 0.45 m × 0.05 m with the order of modes extracted up to (—)8 × 8, (- -)10 × 10, (–)18 × 18 and (- -)25 × 25.

C. A COMPARISON OF IDENTIFICATION RESULTS BY FISTA AND TIKHONOV REGULARIZATION AT 400HZ

Detailed set-up for the simulation in this section is as follows: the disturbing source radiates with an amplitude of 0.03 kg/s^2, two piston sources in a large baffle are located at $(0.075, 0.075, 0)$ *m* and $(0.375, 0.375, 0)$ *m*. Fig. 6 indicates the theoretical source velocity field and the comparison of the identified velocity filed on the vibrating surface at 400 Hz by the FISTA and Tikhonov regularization. The location of the piston sources is identified accurately by both methods. However, ghost sources appear on the velocity map reconstructed by the Tikhonov regularization as shown in Fig. 6(c) while the reconstructed results obtained by the FISTA have a high resolution as shown in Fig. 6(b). In order to quantify and make a comparison of the reconstruction accuracy between two methods, the relative error of the identified source velocities is given as:

$$\xi = \frac{\left\| \mathbf{v}_{id} - \mathbf{v}_{ref} \right\|_2}{\left\| \mathbf{v}_{ref} \right\|_2} \times 100\% \qquad (29)$$
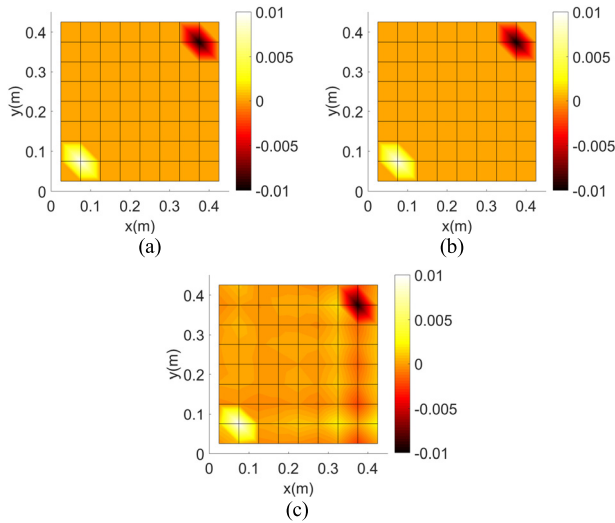
FIGURE 6. Source velocities distribution at 400 Hz (a) theoretical values (b) reconstructed values with ISTA and (c) reconstructed values with Tikhonov regularization.

FIGURE 8. Performance of the iPTF method with FISTA ((a) and (c)) and Tikhonov regularization ((b) and (d)) of the anti-phased sources with different distances.

where $\mathbf{v}_{ref}$ is the reference source velocity and $\mathbf{v}_{id}$ denotes the reconstructed normal velocity of the sources. In Fig. 5, the relative error of the FISTA is 4.42%, much less than 12.06% of the Tikhonov regularization. These results show that the FISTA combining with the iPTF method is able to provide sparser and more accurate results than the iPTF method with Tikhonov regularization.
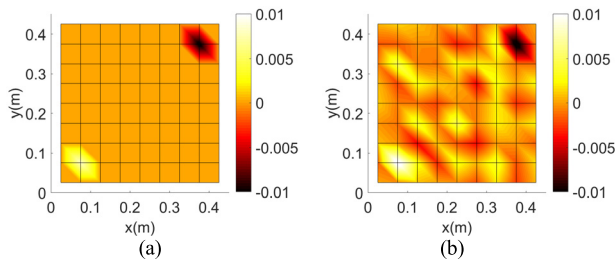

FIGURE 7. Source velocities distribution at 400 Hz with 20dB SNR noise(a) reconstructed values with FISTA (b) reconstructed values with Tikhonov regularization.

Fig. 7 shows the identification results by Tikhonov Regularization and FISTA at 400 Hz in the presence of 20 dB SNR noise. The iPTF method with FISTA provides an excellent identification results with few ghost sources whereas Tikhonov regularization produced much more ghost sources as shown in Fig. 7(b). For both methods, the relative errors have a rise when 20 dB SNR noise exists. The relative error of the FISTA is acceptable with a value of 6.42%. However, the relative error of Tikhonov regularization has a noticeable rise from 12.06% to 29.2%. The comparison shows that the proposed technique that combined the iPTF method with FISTA has great capability to suppress ghost sources and provide accurate reconstructed normal velocities of target sources.
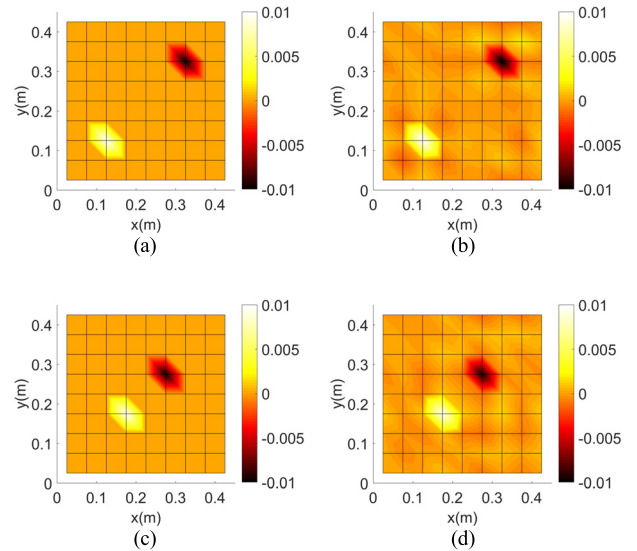
Moreover, as shown in Fig. 8, when the distance between the two sources decreases, the proposed technique still achieves satisfactory results, while many ghost sources appear in the results of the Tikhonov regularization.

D. PERFORMANCE OF THE IPTF METHOD WITH FISTA FOR A FREQUENCY BAND

To show the performance of the iPTF method with FISTA to identify sparsely distributed sources at different frequencies, simulations for a frequency band from 50 Hz to 1000 Hz are conducted in the presence of both the disturbing source and 20 dB SNR noise.
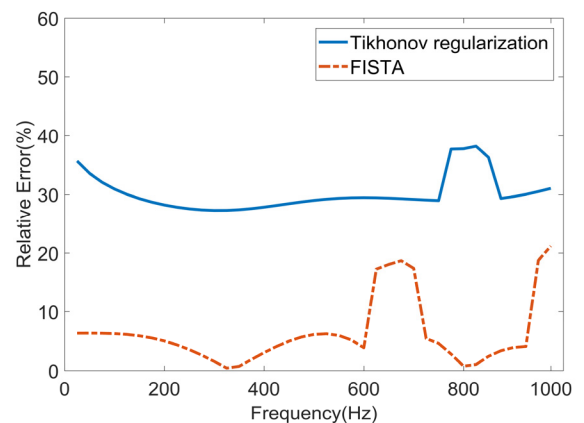

FIGURE 9. Relative errors of the source velocities reconstructed by (-) the iPTF method with Tikhonov regularization and (−·) the iPTF method with FISTA.

Fig. 9 gives the relative errors of identified source normal velocities for the frequency band from 50 Hz to 1000 Hz by the two methods. It is obvious that the relative error of the iPTF with FISTA is lower than that of the iPTF with

Tikhonov regularization for the whole frequency range. And the maximum relative error of the iPTF with FISTA is about 20% which is acceptable for identification, while for most frequencies the relative error is below 10%. On the other hand, relative errors obtained through the Tikhonov regularization are over 30% for most frequencies, with a maximum value up to 40%. For the whole frequency band, the iPTF method with FISTA produces excellent results with high accuracy and sparsity.

The Response Vector Assurance Criterion (RVAC), another parameter to validate the capability of the identification through the frequency band, is given as:

$$\text{RVAC}(\omega) = \sqrt{\frac{\left|\mathbf{v}_{id}(\omega)^H \mathbf{v}_{ref}(\omega)\right|^2}{\left(\mathbf{v}_{id}(\omega)^H \mathbf{v}_{id}(\omega)\right)\left(\mathbf{v}_{ref}(\omega)^H \mathbf{v}_{ref}(\omega)\right)}} \quad (30)$$

where $\mathbf{v}_{id}$ is the identified source velocity, $\mathbf{v}_{ref}$ denoted the theoretical source velocity. RVAC represents the collinearity between two vectors. The RVAC is a value ranging from 1 for perfect correlation to 0 for no correlation. As shown in Fig. 10, the RVAC of the iPTF method with FISTA is above 0.9 within the whole frequency range and reaches 1 for most frequencies, which means that sparse results are obtained with high accuracy. The RVAC calculated by the Tikhonov regularization fluctuates from 0.65 to 0.95, which means the identification results are influenced by ghost sources and cannot provide sparse results like FISTA.
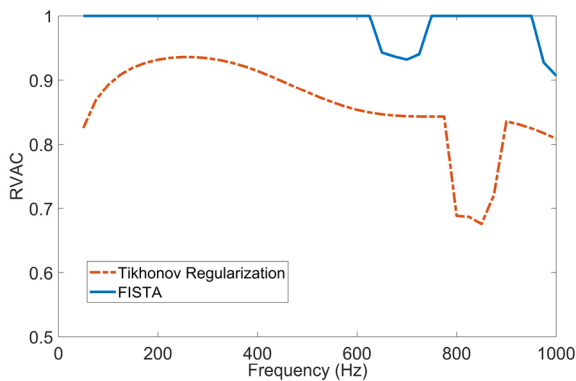

FIGURE 10. RVAC computed between the reference source velocity field identified by (−·) the iPTF method with FISTA and (−) the iPTF method with Tikhonov regularization.

IV. EXPERIMENTS

In order to validate the capability of the proposed technique which combines the iPTF method with FISTA for identifying sparse sources, experiments are conducted in an ordinary room. two loudspeakers (radius of 0.05 m) are embedded in a large wooden baffle (0.6 $m \times$0.6 m), while the size of identification and measurement surface is 0.45 $m \times$0.45 m. Three microphones are utilized to scan the inner and outer hologram surfaces for the pressure measurements. As shown in Fig. 11(a), these microphones are set up parallel to the wooden baffle when measuring the sound pressure of hologram surfaces. In addition, a fourth microphone is used to
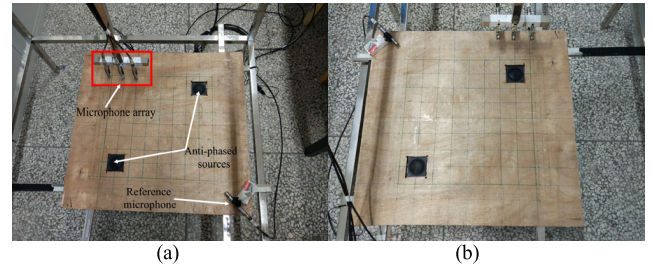

FIGURE 11. Experiment setup and measurements: (a) two loudspeakers, a thick wooden baffle, a reference microphone, and three measurement microphones and (b) diagram of measurements on side hologram surfaces.

acquire a reference signal because the pressure on all of the patches cannot be acquired at the same time. Fig. 11(b) gives the placement of microphones when measuring the pressure of side surfaces. Reflective waves exist in the ordinary room.

Because of the application of double layer measurements to avoid using the p-u probes, pressure measurements are taken on 10 surfaces at 234 points which is the same as the simulation measurement shown in section III-A. The distance between the inner and outer hologram surface in experiments is also set as 0.03m. Once measurements on all measurement surfaces are completed, the sound pressure and particle velocities on the middle surface can be calculated by Equations (13) and (14). The pressure and the velocities will be used to identify the source velocities through both the iPTF with FISTA and Tikhonov regularization. In the identification process, the boundary condition applied to the surfaces of virtual cavity is Neumann boundary condition, which is the same as that used in simulation.
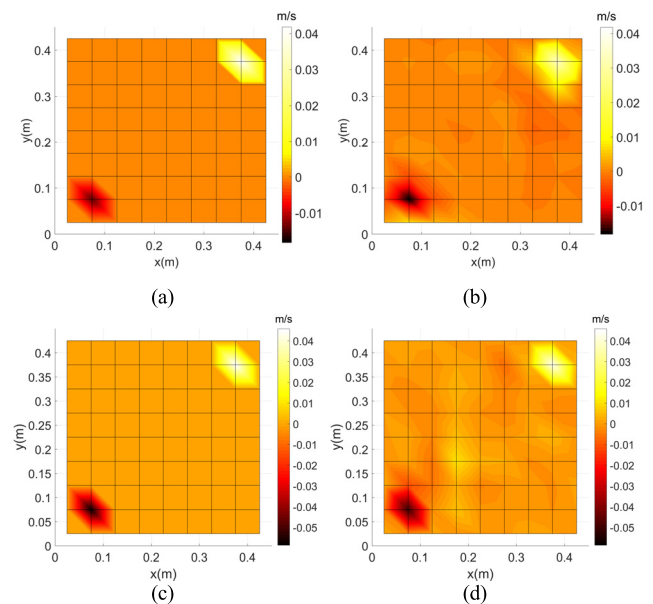

FIGURE 12. Comparison of source velocities identified by the iPTF method with FISTA and Tikhonov regularization respectively at 200 Hz ((a) and (b)) and at 400 Hz ((c) and (d)).

Fig. 12 shows the identified source velocities at 200 Hz and 400 Hz. Fig. 12(a) and (c) gives the results obtained by the

iPTF with Tikhonov regularization. And Fig. 12(b) and (d) shows the identification results obtained by the iPTF with FISTA. Ghost sources appear in the velocity map identified by Tikhonov regularization at both 200 Hz and 400 Hz as the simulation results, while few ghost sources are seen in the identification results of the iPTF method with the FISTA. In addition, the source strength of the two loudspeakers at 200 Hz is different because it is difficult to make the two sources radiate with the same strength. And the reconstruction results exactly reveal that condition. The experimental results confirm the capability of the proposed technique to identify the sparsely distributed sources accurately.

Constrained by experimental conditions, the experiments with two closely distanced loudspeakers are not carried out. However, considering the good agreement between the results in the experiments and previous simulations, it is logical to infer that the proposed technique will give satisfactory results as shown in simulations.

V. CONCLUSION

A technique combining the inverse Patch Transfer Function method (iPTF) with Fast Iterative Shrinkage-Thresholding Algorithm (FISTA) is presented to promote the sparsity of identification results for sparse sources in this paper. Numerical and experimental validation of the iPTF method with FISTA is conducted with two baffled piston sources.

A Neumann evanescent Green's function is utilized to accelerate the convergence of the iPTF method. The double layer measurements are introduced to acquire the normal velocity of the hologram surface by using microphones instead of expensive P-U probes. In order to suppress the ghost sources, the iPTF method with FISTA adopts a proximal gradient-based algorithm and a filter process, which improves the sparsity and accuracy of the identification results. Numerical validations are conducted which indicates that the proposed technique improves the performance of the iPTF method when identifying sparse sources compared to the original method with classic Tikhonov regularization. Simulations for a frequency range from 50 to 1000 Hz indicates that the iPTF method with FISTA has a stable performance with a low error in simulations.

Finally, the experiment results show an excellent correlation with the simulation results. Although the experiments with two closely distanced loudspeakers are not carried out, it is logical to infer that the iPTF methods with FISTA will provide satisfactory results in real conditions. The iPTF method with FISTA can be used as a tool for sparsely distributed sources identification.

REFERENCES

[1] J. D. Maynard, E. G. Williams, and Y. Lee, "Nearfield acoustic holography: I. Theory of generalized holography and the development of NAH," *J. Acoust. Soc. Amer.*, vol. 78, no. 4, pp. 1395–1413, Oct. 1985.

[2] W. A. Veronesi and J. D. Maynard, "Nearfield acoustic holography (NAH) II. Holographic reconstruction algorithms and computer implementation," *J. Acoust. Soc. Amer.*, vol. 81, no. 5, pp. 1307–1322, May 1987.

[3] M. R. Bai, "Application of BEM (boundary element method)-based acoustic holography to radiation analysis of sound sources with arbitrarily shaped geometries," *J. Acoust. Soc. Amer.*, vol. 92, no. 1, pp. 533–549, Jul. 1992.

[4] A. Schuhmacher, J. Hald, K. B. Rasmussen, and P. C. Hansen, "Sound source reconstruction using inverse boundary element calculations," *J. Acoust. Soc. Amer.*, vol. 113, no. 1, pp. 114–127, Jan. 2003.

[5] C. Bi, X. Chen, C. Jian, and Z. Rong, "Nearfield acoustic holography based on the equivalent source method," *Sci. China Ser. E Eng. Mater. Sci.*, vol. 48, no. 3, p. 338, 2005.

[6] Z. Chu, G. Ping, P. Cai, Y. Yang, and C. Chen, "Application of Bayesian regularization criterion in near field acoustic holography based on equivalent source method," *Noise Vib. Worldwide*, vol. 46, no. 6, pp. 20–28, Jun. 2015.

[7] Z. Wang and S. F. Wu, "Helmholtz equation-least-squares method for reconstructing the acoustic pressure field," *J. Acoust. Soc. Amer.*, vol. 102, no. 4, pp. 2020–2032, Oct. 1997.

[8] J. Hald, "Basic theory and properties of statistically optimized near-field acoustical holography," *J. Acoust. Soc. Amer.*, vol. 125, no. 4, pp. 2105–2120, Apr. 2009.

[9] F. Jacobsen, X. Chen, and V. Jaud, "A comparison of statistically optimized near field acoustic holography using single layer pressure-velocity measurements and using double layer pressure measurements," *J. Acoust. Soc. Amer.*, vol. 123, no. 4, pp. 1842–1845, Apr. 2008.

[10] F. Jacobsen and V. Jaud, "Statistically optimized near field acoustic holography using an array of pressure-velocity probes," *J. Acoust. Soc. Amer.*, vol. 121, no. 3, pp. 1550–1558, Mar. 2007.

[11] M. Aucejo, N. Totaro, and J.-L. Guyader, "Identification of source velocities on 3D structures in non-anechoic environments: Theoretical background and experimental validation of the inverse patch transfer functions method," *J. Sound Vibrat.*, vol. 329, no. 18, pp. 3691–3708, Aug. 2010.

[12] N. Totaro, D. Vigoureux, Q. Leclère, J. Lagneaux, and J. Guyader, "Sound fields separation and reconstruction of irregularly shaped sources," *J. Sound Vibrat.*, vol. 336, pp. 62–81, Feb. 2015.

[13] D. Vigoureux, N. Totaro, J. Lagneaux, and J.-L. Guyader, "Inverse patch transfer functions method as a tool for source field identification," *J. Vibrat. Acoust.*, vol. 137, no. 2, Apr. 2015, Art. no. 021006.

[14] S. Forget, N. Totaro, J. Guyader, and M. Schaeffer, "Source fields reconstruction with 3D mapping by means of the virtual acoustic volume concept," *J. Sound Vibrat.*, vol. 381, pp. 48–64, Oct. 2016.

[15] S. Xiang, W. Jiang, and S. Pan, "Sound source identification in a noisy environment based on inverse patch transfer functions with evanescent green's functions," *J. Sound Vibrat.*, vol. 359, pp. 68–83, Dec. 2015.

[16] S. Yoon and P. Nelson, "Estimation of acoustic source strength by inverse methods: Part II, experimental investigation of methods for choosing regularization parameters," *J. Sound Vibrat.*, vol. 233, no. 4, pp. 665–701, Jun. 2000.

[17] E. G. Williams, "Regularization methods for near-field acoustical holography," *J. Acoust. Soc. Amer.*, vol. 110, no. 4, pp. 1976–1988, Oct. 2001.

[18] J. Hald, "Fast wideband acoustical holography," *J. Acoust. Soc. Amer.*, vol. 139, no. 4, pp. 1508–1517, Apr. 2016.

[19] J. Hald, "A comparison of iterative sparse equivalent source methods for near-field acoustical holography," *J. Acoust. Soc. Amer.*, vol. 143, no. 6, pp. 3758–3769, Jun. 2018.

[20] H. F. Alqadah, N. Valdivia, and E. G. Williams, "A super-resolving near-field electromagnetic holographic method," *IEEE Trans. Antennas Propag.*, vol. 62, no. 7, pp. 3679–3692, Jul. 2014.

[21] T. Suzuki, "L1 generalized inverse beam-forming algorithm resolving coherent/incoherent, distributed and multipole sources," *J. Sound Vibrat.*, vol. 330, no. 24, pp. 5835–5851, Nov. 2011.

[22] A. Beck and M. Teboulle, "A fast iterative shrinkage-thresholding algorithm for linear inverse problems," *SIAM J. Imag. Sci.*, vol. 2, no. 1, pp. 183–202, Jan. 2009.

[23] H. Nélisse and J. Nicolas, "Characterization of a diffuse field in a reverberant room," *J. Acoust. Soc. Amer.*, vol. 101, no. 6, pp. 3517–3524, Jun. 1997.

[24] P. Nelson and S. Yoon, "Estimation of acoustic source strength by inverse methods: Part I, conditioning of the inverse problem," *J. Sound Vibrat.*, vol. 233, no. 4, pp. 639–664, Jun. 2000.

[25] M. Ouisse, L. Maxit, C. Cacciolati, and J.-L. Guyader, "Patch transfer functions as a tool to couple linear acoustic problems," *J. Vibrat. Acoust.*, vol. 127, no. 5, pp. 458–466, Oct. 2005.

LINGYU LOU received the bachelor's degree in vehicle engineering from Chongqing University, Chongqing, China, in 2017, where he is currently pursuing the master's degree. His current research interests include signal processing for acoustical imaging, broadband acoustical measurement, and noise control.

ZHONGMING XU received the B.Eng. degree in vehicle engineering from Chongqing University, China, in 1983, the master's degree from Tsinghua University, China, in 1992, and the Ph.D. degree from The University of Tokyo, Japan, in 2002. He is currently a Researcher with the State Key Laboratory of Mechanical Transmission and a Professor with the School of Automotive Engineering, Chongqing University. His current research interest is noise and vibration control.

LINSEN HUANG received the bachelor's degree in vehicle engineering from the Inner Mongolia University of Technology, Inner Mongolia, China, in 2015, and the master's degree in mechanical engineering from Guizhou University, Guizhou, China, in 2018. He is currently pursuing the Ph.D. degree with Chongqing University. His current research interests include signal processing for acoustical imaging, broadband acoustical measurement, and noise control.

ZHIFEI ZHANG received the B.Eng., master's and Ph.D. degrees in vehicle engineering from Chongqing University, China, in 2003, 2005, and 2008, respectively. He was a Visiting Scholar with the University of Southampton, U.K., from 2014 to 2015. He is currently a Vice Professor with the School of Automotive Engineering, Chongqing University. His research interests include acoustic measurement and noise control.

YANSONG HE received the B.Eng. and master's degrees in automotive from Chongqing University, China, in 1990 and 1993, respectively, and the Ph.D. degree in solid mechanics from Chongqing University, in 2003. He was a Visiting Scholar in U.S., from 2004 to 2005. He is currently a Professor with the School of Automotive Engineering. His research interest includes mechanics and control of noise and vibration.

● ● ●